Piezoelectric Nanoparticle-Assisted Wireless Neuronal Stimulation

Attilio Marino,[*,†,‡] Satoshi Arai,[§] Yanyan Hou,[§] Edoardo Sinibaldi,[†] Mario Pellegrino,[⊥] Young-Tae Chang,[∥,#] Barbara Mazzolai,[†] Virgilio Mattoli,[†] Madoka Suzuki,[*,§,▽] and Gianni Ciofani[*,†]

[†]Center for Micro-BioRobotics, Istituto Italiano di Tecnologia, Viale Rinaldo Piaggio 34, 56025 Pontedera (Pisa), Italy, [‡]The Biorobotics Institute, Scuola Superiore Sant'Anna, Viale Rinaldo Piaggio 34, 56025 Pontedera (Pisa), Italy, [§]WASEDA Bioscience Research Institute in Singapore (WABIOS), Biopolis Way 11, #05-02 Helios, 138667 Singapore, [⊥]Dipartimento di Ricerca Traslazionale e delle Nuove Tecnologie in Medicina e Chirurgia, University of Pisa, Via Savi 10, 56126 Pisa, Italy, [∥]Department of Chemistry, National University of Singapore, MedChem Program of Life Sciences Institute, National University of Singapore, 3 Science Drive 3, 117543 Singapore, [#]Laboratory of Bioimaging Probe Development, Singapore Bioimaging Consortium, Agency for Science, Technology and Research (A*STAR), Biopolis, 138667 Singapore, and [▽]Organization for University Research Initiatives, Waseda University, #304, Block 120-4, 513 Waseda-Tsurumaki-Cho, Shinjuku-Ku, 162-0041 Tokyo, Japan

ABSTRACT Tetragonal barium titanate nanoparticles (BTNPs) have been exploited as nanotransducers owing to their piezoelectric properties, in order to provide indirect electrical stimulation to SH-SY5Y neuron-like cells. Following application of ultrasounds to cells treated with BTNPs, fluorescence imaging of ion dynamics revealed that the synergic stimulation is able to elicit a significant cellular response in terms of calcium and sodium fluxes; moreover, tests with appropriate blockers demonstrated that voltage-gated membrane channels are activated. The hypothesis of piezoelectric stimulation of neuron-like cells was supported by lack of cellular response in the presence of cubic nonpiezoelectric BTNPs, and further corroborated by a simple electroelastic model of a BTNP subjected to ultrasounds, according to which the generated voltage is compatible with the values required for the activation of voltage-sensitive channels.

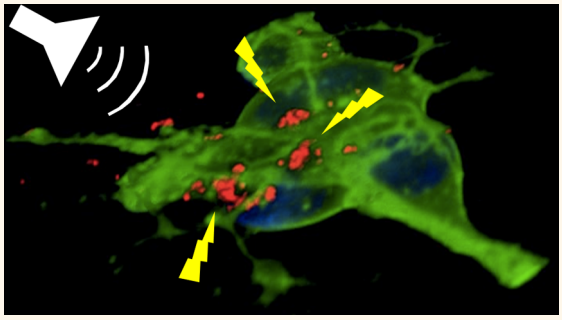

KEYWORDS: barium titanate nanoparticles · ultrasounds · piezoelectricity · SH-SY5Y cells · calcium imaging

The possibility to stimulate/modulate the neural activity is often limited by the restricted accessibility of the nervous system,[1] and several innovative techniques are being explored in order to address this challenge. Among these, the rapid development of genetically encoded actuators/sensors, *i.e.*, optogenetics,[2] is allowing for the detailed investigation of the mechanisms of various diseases, especially those presenting a neuronal etiology, in different animal models, thanks to a fine cell activity modulation/monitoring.[3−7] However, the exploitation of optogenetics is currently limited by several complications, including the phototoxicity[8] and the scarce penetration of the light through the tissues due to their opacity at the suitable wavelengths.[9] Other well-characterized neural stimulation approaches are represented by the deep brain stimulation (DBS),[10] the trans-cranial direct current stimulation (tDCS),[11,12] and the trans-cranial magnetic stimulation (TMS).[13] Drawbacks of DBS are the necessity of an invasive surgical operation, followed by inflammation and gliosis at the implant site, while the main disadvantage of the tDCS and TMS is the low spatial resolution (a brain volume of about 1 cm in diameter).

Ultrasounds (US) can be instead exploited for trans-cranial stimulation without the requirement of surgical processes, and with a resolution of about 3 mm,[14] which can be further improved by the use of hyperlenses and acoustic metamaterials.[15,16] However, the heterogeneous results obtained with the US stimulation, that in certain conditions may induce neural silencing rather than excitation, are influenced by the physical parameters of the US, including frequency and power. Recently, Tufail *et al.* reported an exhaustive summary of the US-mediated neuromodulation effects observed by using different US parameters and different neural models.[17]

US can be exploited in combination with piezoelectric materials in order to generate direct-current output:[18,19] indeed, piezoelectric materials are able to efficiently

* Address correspondence to attilio.marino@iit.it, suzu_mado@aoni.waseda.jp, gianni.ciofani@iit.it.

Received for review May 26, 2015 and accepted July 13, 2015.

Published online July 13, 2015
10.1021/acsnano.5b03162

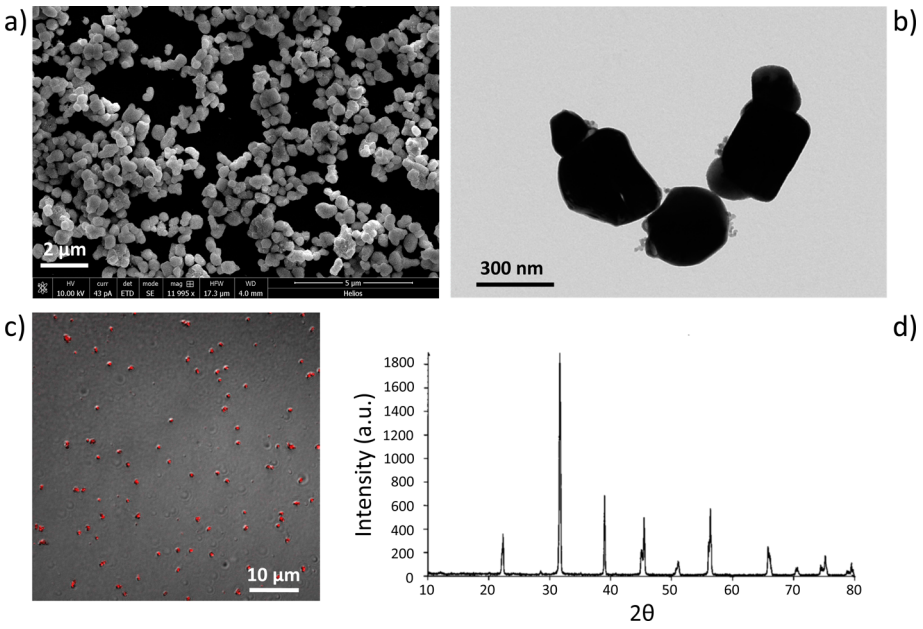

Figure 1. Barium titanate nanoparticles (BTNPs) characterized by a tetragonal crystalline structure. SEM (a), TEM (b) and confocal fluorescence (c) imaging of BTNPs. In (c), confocal fluorescence image (red) is merged with the transmitted light image (gray) of the same field of view. The crystallographic structure revealed thanks to the XRD analysis shows two close peaks at $2\theta = 44.85°$ and $2\theta = 45.38°$, specific of the tetragonal configuration of the crystal (d).

generate electricity in response to the US mechanical stimulations. Taking advantage of the piezoelectricity of different nanomaterials, such as ZnO nanowires and $BaTiO_3$ nanoparticles (BTNPs), it is possible to obtain US-driven nanogenerators able to generate output currents inside biological liquid for energy harvesting and for self-powered electronics.[20−22] In a previous work of our group, the US-driven piezoelectric stimulation of PC12 neural-like cells was performed for the first time by using boron nitride nanotubes (BNNTs).[23] In this work, a significant enhancement of the neurite outgrowth was observed in response to the combined US + BNNT stimulus, with respect to the US stimulus without the presence of the piezoelectric nanoparticles; moreover, the significant increase of the neurite length dependent by the US + BNNT stimulation was suggested to be mediated by a Ca^{2+} influx. However, the impossibility to perform electrophysiological recordings in conjunction with the US stimulation has not allowed the mechanisms giving rise the Ca^{2+} influx (*i.e.*, piezoelectric-mediated plasma membrane depolarization) to be investigated, and consequently the different ion currents involved to be elucidated.

In this work, we carried out neural stimulation with US and piezoelectric BTNPs characterized by a tetragonal crystalline configuration, and the effects of both US and US + BTNP stimulations on SH-SY5Y-derived neurons were deeply investigated, by exploiting imaging techniques for detecting the Ca^{2+}/Na^{+} fluxes and temperature levels. Our results show as the stimulation with US + piezoelectric BTNPs was able to induce tetrodotoxin (TTX) and cadmium (Cd^{2+}) sensitive high-amplitude Ca^{2+} transients, and that the observed transients are specifically evoked thanks to the piezoelectric properties of these nanoparticles with single cell resolution. Our findings thus strongly support the hypothesis that the piezoelectric stimulation is able to induce a Ca^{2+} influx, which likely mediates the enhancement of the neurite outgrowth and neural differentiation,[23,24] and suggest the possible use of this approach as a wireless tool to modulate neuronal activity even deeply *in vivo*, by a combination of piezoelectric nanoparticles and a pulse of ultrasounds.

RESULTS

Tetragonal Barium Titanate Nanoparticle Characterization. Images of the BTNPs used in this work, wrapped with gum Arabic, are provided in Figure 1a (scanning electron microscopy, SEM) and Figure 1b (transmission electron microscopy, TEM). These observations revealed quite well-dispersed structures, with some aggregates of a few nanoparticles. The hydrodynamic size of the BTNPs, measured through dynamic light scattering (DLS), resulted of 479.0 ± 145.3 nm, with a polydispersity index of 0.180. The *Z*-potential was −40.4 ± 5.2 mV, highlighting an excellent stability of the dispersion. Hydrodynamic size and *Z*-potential were evaluated also in experimental conditions (50 μg/mL of BTNPs in artificial cerebrospinal fluid) and resulted 573.3 ± 173.8 nm and −17.2 ± 1.2 mV, respectively. Most useful for tracking in cell experiments, BTNPs resulted visible through confocal fluorescence imaging (Figure 1c), by using an excitation at 633 nm and a collection from 645 to 745 nm. From XRD analysis (Figure 1d), BTNPs resulted to have a perovskite-like crystallographic structure. Tetragonal phase of

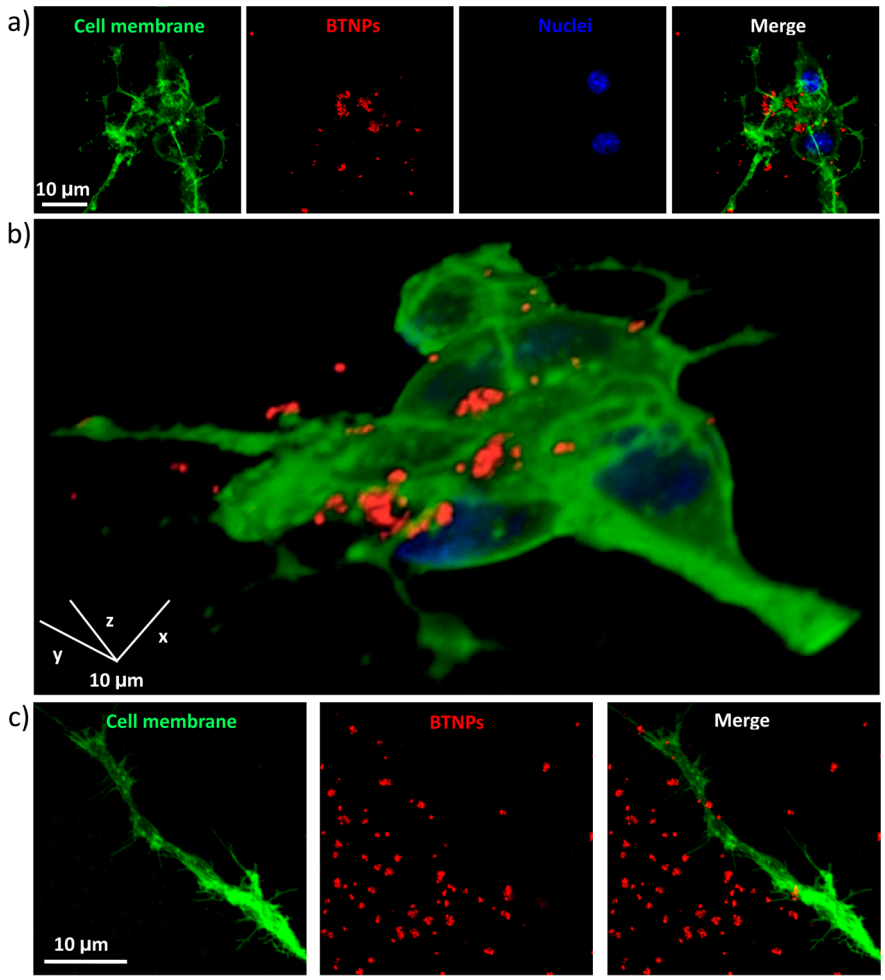

Figure 2. Confocal fluorescence microscopy of BTNPs associating to the neuronal plasma membranes. (a) Characteristic confocal *z*-stack of BTNP-treated SH-SY5Y-derived neurons (neuronal plasma membranes in green, BTNPs in red and nuclei in blue). (b) 3D rendering of the confocal *z*-stacks of the same field as in (a). BTNPs were also detected associating to the neurite membranes (c).

$BaTiO_3$, typical of piezoelectric nanoparticles, was detected, with two close peaks at $2\theta = 44.85°$ and $2\theta = 45.38°$.[25]

US-Driven BTNP Stimulation Induces Ca^{2+} Transients. In order to evaluate the BTNPs/neurons interaction, confocal fluorescence microscopy was carried out (Figure 2). Particularly, high amount of BTNPs (in red) was observed associated with the plasma membrane (in green) of the SH-SY5Y-derived neurons after 24 h from the BTNP treatment (Figure 2a); Figure 2b depicts the 3D rendering of a confocal *z*-stack acquisition (see also Video S1, provided as Supporting Information). From all these observations, we can conclude as nanoparticles are mainly associated with the plasma membrane without a significant cellular internalization. Finally, BTNPs were observed associated not only to the membrane of the SH-SY5Y cell bodies, but also to their neurites, as shown by Figure 2c.

Cellular viability following the experimental procedures was confirmed by WST-1 metabolic activity assay and propidium iodide staining, the latter evaluating the integrity of the cellular membrane after the stimulation. Four experimental groups were considered: control cultures, cultures treated with BTNPs (50 μg/mL), cultures treated with US (0.8 W/cm^2), and cultures treated with both BTNPs (50 μg/mL) and US (0.8 W/cm^2). Results are provided in Figure S1 as Supporting Information, and highlight no statistically significant differences among the different treatments in terms of both metabolic activity (Figure S1a, evaluated after 24 h since the stimulation) and membrane integrity (Figure S1b, evaluated immediately after the stimulation in order to highlight also temporarily phenomena of membrane permeabilization).

After the evaluation of the BTNP/cell interactions at the level of the plasma membrane, we monitored the intracellular Ca^{2+} dynamics in response to the US stimulation performed at different intensities (0.1, 0.2, 0.4 and 0.8 W/cm^2), with or without BNTPs (Figure 3). Interestingly, we observed that, by stimulating SH-SY5Y-derived neurons with BTNPs + US at 0.8 W/cm^2, it was possible to activate high-amplitude Ca^{2+} transients ($\Delta F/F_0$ peak = 0.62 ± 0.12), significantly higher with respect to the low-amplitude Ca^{2+} transients

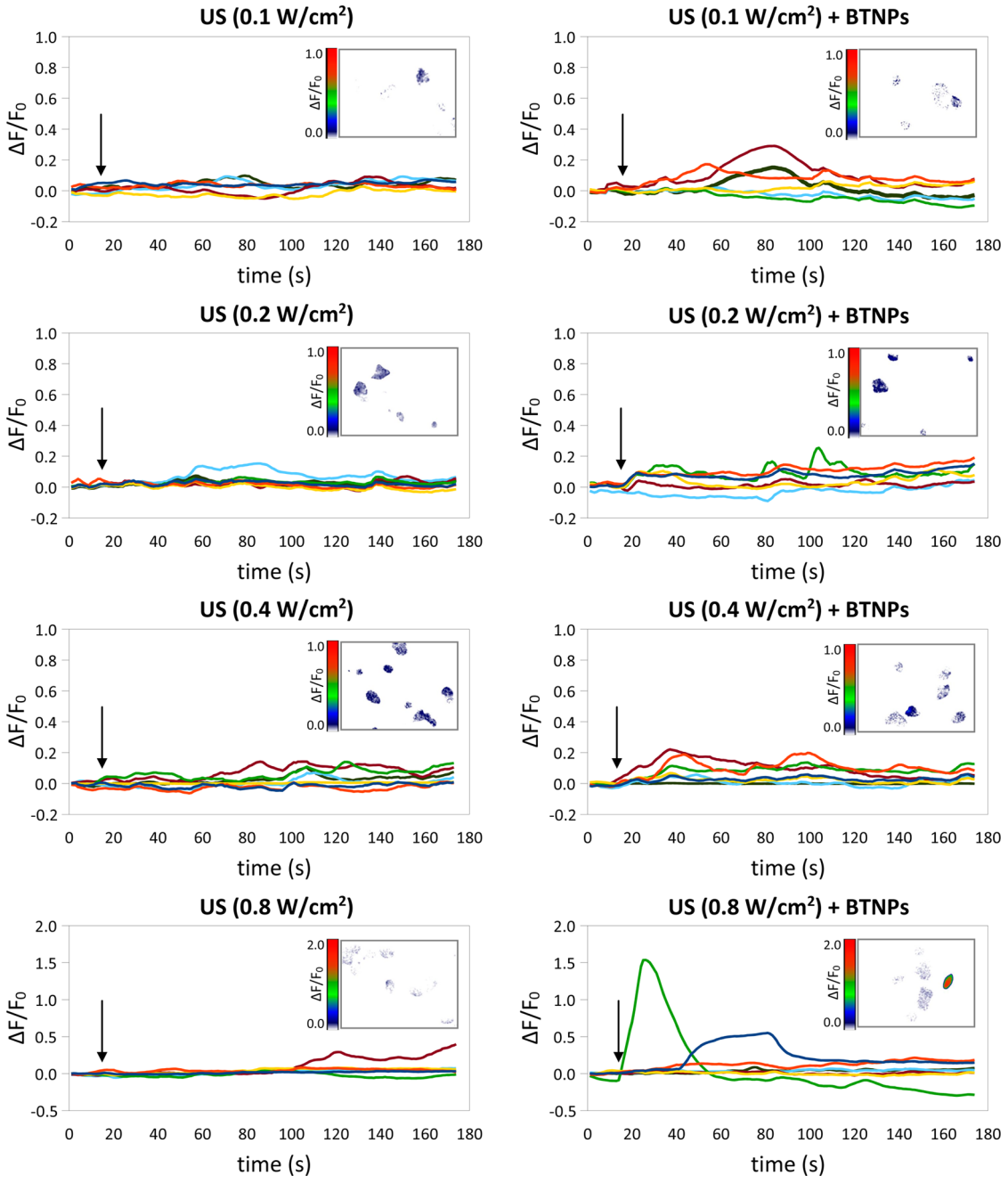

Figure 3. Calcium imaging of SH-SY5Y-derived neurons in response to the US stimulation performed at different intensities (0.1, 0.2, 0.4 and 0.8 W/cm^2), with or without BNTPs: time courses of the $\Delta F/F_0$ traces. Arrows indicate the moment when the 5-s US pulse was initiated; in the inlet of each graph a representative calcium imaging time-lapse frame is reported (at t = 30).

detected in all the other conditions ($p < 0.05$), including the treatment with US at 0.8 W/cm^2 but without BTNPs ($\Delta F/F_0$ peak = 0.15 ± 0.04; please refer to the Table 1 for the comparison of all of the peak amplitudes). Concerning the tests performed with US intensities < 0.8 W/cm^2, no significant differences in terms of calcium transients amplitude evoked by US + BTNPs were found with respect to the plain US stimulation ($p > 0.05$). In the following results, relative to the investigation of the mechanisms at the base of the observed phenomenon, just the stimulation at the highest intensity (0.8 W/cm^2) will be thus considered. Video S2, provided as Supporting Information, shows the Ca^{2+} imaging time-lapse course (18X accelerated) performed on cultures stimulated with US (0.8 W/cm^2) in the presence of BTNPs. The US stimulation was applied at t_{video} = 1 s.

In order to investigate the ion channels involved in the observed Ca^{2+} transients, Ca^{2+} imaging experiments were performed in the presence of blockers either of the voltage-gated Ca^{2+} channels (Cd^{2+}) or of the voltage-gated Na^+ channels (TTX) (Figure 4).[26,27] Figure 4a–d are representative $\Delta F/F_0$ traces relative to Ca^{2+} imaging time-lapses of neurons stimulated by US, US + BTNPs, Cd^{2+} + US + BTNPs, and TTX + US + BTNPs, respectively;

in the inlet of each graph a representative Ca^{2+} imaging time-lapse frame is reported (more time-lapse images are reported in Figure S2 as Supporting Information). In Figure 4a we can appreciate low-amplitude Ca^{2+} transients ($\Delta F/F_0$ peak = 0.15 ± 0.04) induced by the US stimulus. In Figure 4b, the US in the presence of BTNPs induce significantly higher Ca^{2+} peaks ($\Delta F/F_0$ peak = 0.62 ± 0.12; $p < 0.05$) compared to the US stimulation without nanoparticles. These high-amplitude Ca^{2+} transients were suppressed by both the Cd^{2+} (Figure 4c) and the TTX (Figure 4d) treatments. In both conditions (Cd^{2+} + US + BTNPs and TTX + US + BTNPs) we detected low-amplitude Ca^{2+} peaks ($\Delta F/F_0$ peak = 0.16 ± 0.02 in the presence of Cd^{2+} and $\Delta F/F_0$ peak = 0.14 ± 0.01 in the presence of TTX), similar to those observed by stimulating with US without BTNPs ($\Delta F/F_0$ peak = 0.15 ± 0.04; $p > 0.05$; Table 1), thus suggesting that the induction of the high-amplitude Ca^{2+} transients by the US + BTNPs stimulation is mediated by both Ca^{2+} and Na^+ voltage-gated channels.

TABLE 1. Calcium/Sodium Transient Amplitude (In Terms of $\Delta F/F_0$ Peak Average ± Standard Error) Measured in Response to the Different Stimulations and Treatments

calcium imaging			
treatment		**US**	**US + BTNPs**
0.1 W/cm^2		No transients	0.14 ± 0.03
0.2 W/cm^2		0.09 ± 0.02	0.15 ± 0.02
0.4 W/cm^2		0.16 ± 0.02	0.22 ± 0.04
0.8 W/cm^2		0.15 ± 0.04	0.62 ± 0.12
0.8 W/cm^2	Cd^{2+}	N/A	0.16 ± 0.02
	TTX	N/A	0.14 ± 0.01
	EGTA	0.16 ± 0.04	0.12 ± 0.03
	thapsigargin + EGTA	no transients	no transients
	gentamicin	0.15 ± 0.05	0.78 ± 0.24
	cubic crystal	0.15 ± 0.04	0.12 ± 0.01

sodium imaging			
treatment		**US**	**US + BTNPs**
0.8 W/cm^2		no transients	0.032 ± 0.001
0.8 W/cm^2	Cd^{2+}	N/A	0.011 ± 0.001
	TTX	N/A	no transients

US-Driven BTNP Stimulation Induces TTX-Sensitive Na^+ Transients. Possible effects of the stimulation on the Na^+ fluxes were evaluated by performing Na^+ imaging experiments on SH-SY5Y-derived neurons treated with US, US + BTNPs, Cd^{2+} + US + BTNPs, and TTX + US + BTNPs. Representative $\Delta F/F_0$ traces relative to Na^+ imaging time-lapses are shown in Figure 5a–d; in the inlet of each graph a representative Na^+ imaging time-lapse frame is reported (more time-lapse images are reported in Figure S3 as Supporting Information). The US stimulation without BTNPs was not able to induce any appreciable Na^+ peak (Figure 5a), while a Na^+ transient was clearly detected in response to the US + BTNP activation ($\Delta F/F_0$ peak = 0.032 ± 0.001; Figure 5). Na^+ peaks of lower amplitude were revealed by stimulating SH-SY5Y-derived neurons with US + BTNPs in the presence of the voltage-gated Ca^{2+} channel blocker Cd^{2+} ($\Delta F/F_0$ peaks =0.011 ± 0.001; Figure 5c),

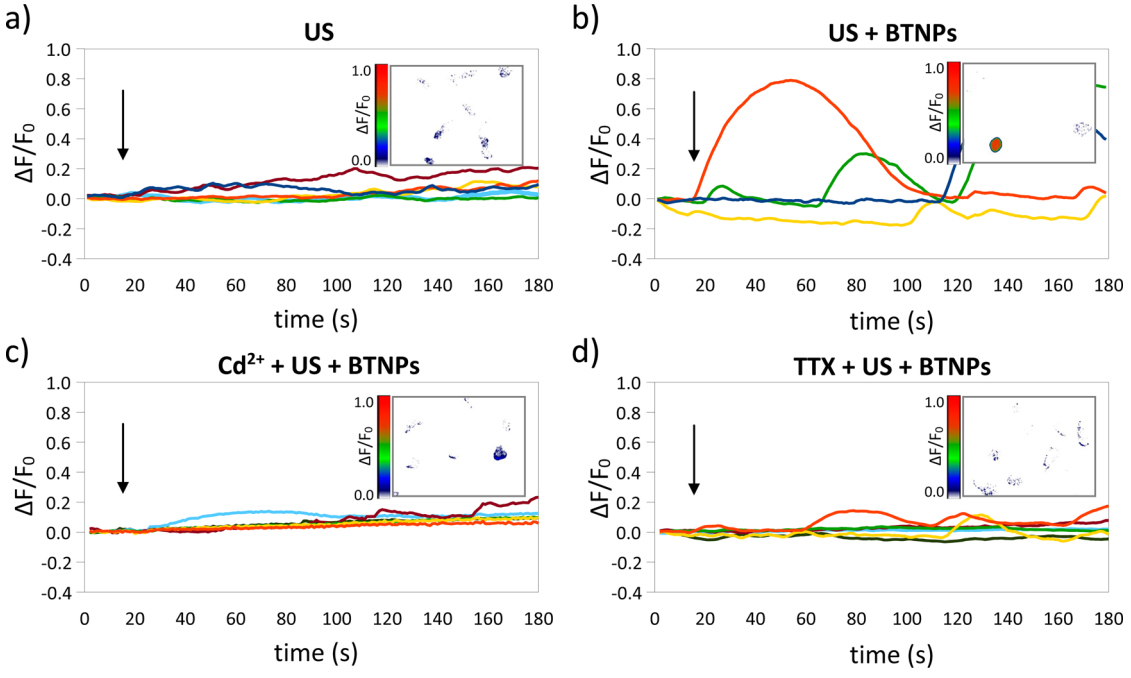

Figure 4. US + BTNP stimulation (0.8 W/cm^2) evokes Cd^{2+} and TTX-sensitive calcium transients. Representative $\Delta F/F_0$ traces relative to calcium imaging time-lapses of SH-SY5Y-derived neurons stimulated by US (a), US + BTNPs (b), US + BTNPs in the presence of Cd^{2+} (c) or TTX (d). Arrows indicate the moment when the 5-s US pulse was initiated; in the inlet of each graph a representative calcium imaging time-lapse frame is reported (at t = 50).

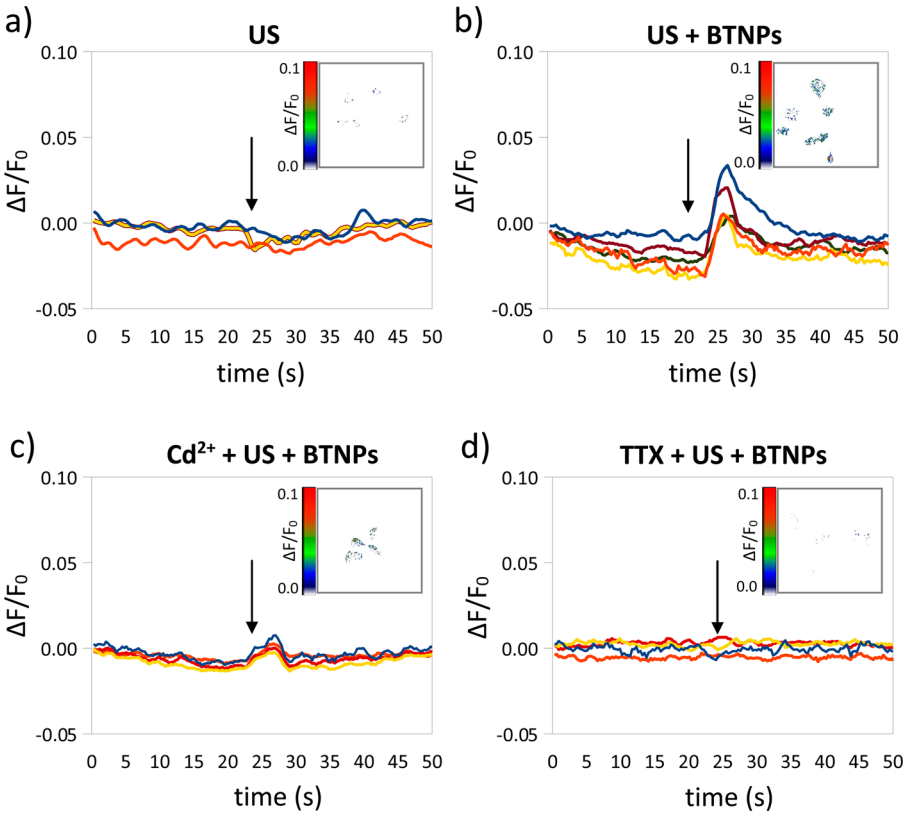

Figure 5. US + BTNP stimulation (0.8 W/cm^2) induces TTX-sensitive sodium transients. Representative $\Delta F/F_0$ traces relative to sodium imaging time-lapses of SH-SY5Y-derived neurons stimulated by US (a), US + BTNPs (b), US + BTNPs in the presence of Cd^{2+} (c) or TTX (d). Arrows indicate the moment when the 5-s US pulse was initiated; in the inlet of each graph a representative sodium imaging time-lapse frame is reported (at t = 27).

while no peaks were detected in the TTX treatment (Figure 5d).

Investigation of Ca^{2+} Sources Involved in the US-Driven BTNP Stimulation. The Ca^{2+} sources involved in the stimulations, *e.g.*, intracellular stores and/or extracellular environment, were investigated as reported in Figure 6 (in the inlet of each graph a representative Ca^{2+} imaging time-lapse frame is reported; more time-lapse images are reported in Figure S4 as Supporting Information). The US stimulation in Ca^{2+}-free conditions (and in the presence of 5 mM of the Ca^{2+} chelator ethylene glycol tetraacetic acid, EGTA) induced low-amplitude Ca^{2+} transients ($\Delta F/F_0$ peak = 0.16 ± 0.04; Figure 6a), non-significantly different from those observed in standard conditions, *i.e.*, in the presence of 2 mM extracellular Ca^{2+} ($\Delta F/F_0$ peak = 0.15 ± 0.04; $p > 0.05$; Figure 4a). This result suggests that the intracellular Ca^{2+} stores are implicated in the low-amplitude Ca^{2+} transients observed during the stimulations with US, but not in the presence of BTNPs. Interestingly, we also observed low-amplitude Ca^{2+} transients when stimulating with BTNPs and US in the EGTA-supplemented Ca^{2+}-free medium ($\Delta F/F_0$ peak = 0.12 ± 0.03; Figure 6b). This low-amplitude peak is significantly lower compared to the high amplitude peak measured in standard conditions (*i.e.*, 2 mM of extracellular Ca^{2+}; $\Delta F/F_0$ peak = 0.62 ± 0.12; $p < 0.05$; Table1), suggesting that the US + BTNP stimulation, conversely to the plain US stimulation, is able to activate the Ca^{2+} influx through the plasma membrane. This result is in agreement with the previous observation highlighting that the high-amplitude peaks are inhibited by the treatments with TTX and Cd^{2+}, which are blockers of the cell membrane voltage-gated channels.[26,27] Further study suggests that the source of these low-amplitude Ca^{2+} transients is the endoplasmic reticulum (ER): both the low-amplitude peaks reported after the plain US (Figure 6c) and the US + BTNP (Figure 6d) stimulation in extracellular Ca^{2+}-free conditions completely disappear by depleting the Ca^{2+} flux from ER with thapsigargin, suggesting that the ER represents the involved Ca^{2+} store.

Thermal Effects of the US-Driven BTNP Stimulation. US stimulations higher than 0.5 W/cm^2 are known to locally increase the temperature,[17,28,29] and the ER is prone to release Ca^{2+} in response to a heat pulse.[30,31] We therefore investigated whether the US and US + BTNP stimuli are able to induce a temperature increment at ER level (Figure S5, supplied as Supporting Information). In order to monitor the ER temperature during the stimulations, we took advantage of a thermosensitive fluorescent dye able to specifically target the ER, the ER thermo yellow.[32] In Figure S5a we can appreciate the colocalization of the fluorescence

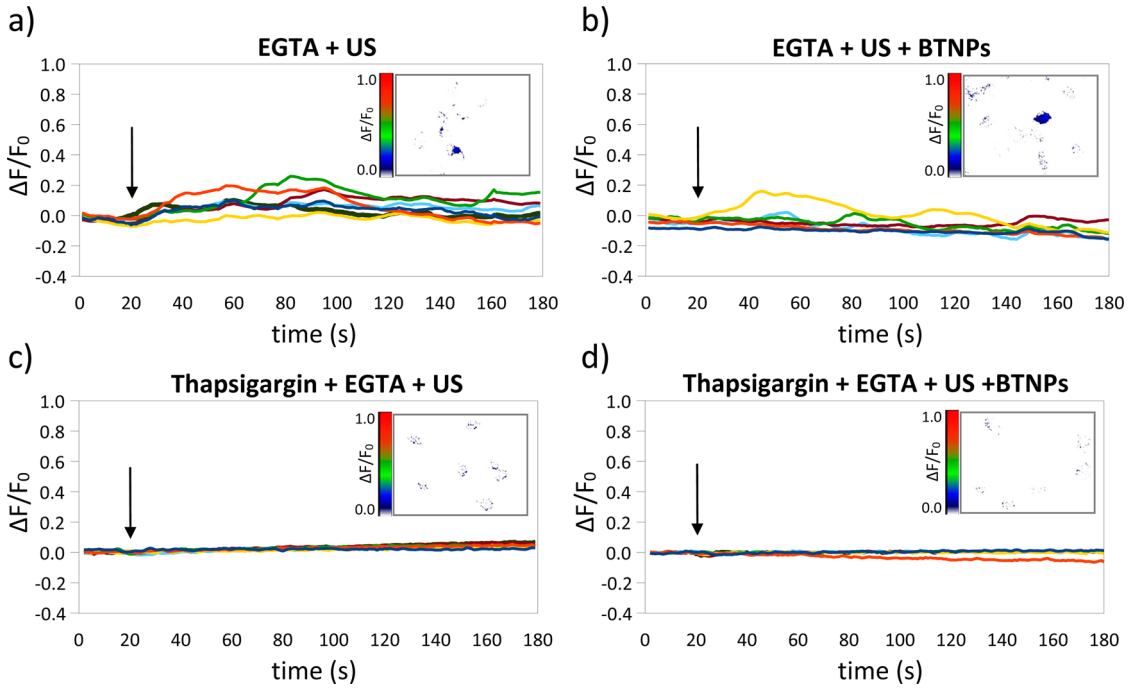

Figure 6. Calcium sources involved during US and US + BTNP stimulations (0.8 W/cm^2). Representative $\Delta F/F_0$ traces relative to calcium imaging time-lapses of SH-SY5Y-derived neurons in calcium-free conditions stimulated by US (a) and US + BTNPs (b) show in both case low-amplitude calcium transients. Observed transients were completely hindered by depleting the Ca^{2+} flux from the endoplasmic reticulum with thapsigargin before both the US (c) and US + BTNP (d) stimulations. Arrows indicate the moment when the 5-s US pulse was initiated; in the inlet of each graph a representative calcium imaging time-lapse frame is reported (at t = 50).

signal stemming from the ER thermo yellow with that one of the ER tracker, demonstrating the high specificity of the ER thermo yellow in SH-SY5Y cells. The sensitivity of the ER thermo yellow in SH-SY5Y cells was determined to be −2.0%/°C by linearly fitting the F/F_0 data measured at different ER temperature increment (ΔT, °C) starting from the room temperature (Figure S5b). Figure S5c and S5d show representative time courses of the ER thermometer fluorescence signal during the stimulation with US (0.8 W/cm^2) and with US + BTNPs, respectively. The relative ΔT (°C) traces are shown in Figure S5e and S5f, showing that the US stimulation is able to increase the ER temperature both in presence (1.66 ± 0.30 °C) and in absence (1.68 ± 0.31 °C) of BTNPs, but without any significant difference between the two conditions ($p > 0.05$).

Further Evaluations of the Mechanisms at the Base of the US-Driven BTNP Stimulation. The role of mechanosensitive channels in the low-amplitude and high-amplitude Ca^{2+} transients respectively observed after the US and US + BTNP stimulations was investigated by perfoming Ca^{2+} imaging experiments in the presence of 200 μM gentamicin, a blocker of mechano-sensitive cation channels that does not affect the voltage-gated Ca^{2+} currents.[33−35] Even in the presence of gentamicin, low-amplitude ($\Delta F/F_0$ peak = 0.15 ± 0.05) and high-amplitude ($\Delta F/F_0$ peak = 0.78 ± 0.24; $p < 0.05$) Ca^{2+} peaks were respectively detected after the US (Figure 7a) and the US + BTNP stimulations (Figure 7b), suggesting that the mechano-sensitive cation channels are not at the base of the mechanism describing the effects observed during the stimulations.

Finally, in order to investigate whether the high-amplitude Ca^{2+} transients observed in the US + BTNP stimulation are indeed due to a piezoelectric effect, we performed stimulation in the presence of BTNPs characterized by a cubic crystalline configuration (Figure 7c), and thus not piezoelectric.[25] Interestingly, we observed that in this case the US + BTNP stimulation was able to induce only low-amplitude Ca^{2+} transients ($\Delta F/F_0$ peak = 0.12 ± 0.01), not significantly different to those observed after the plain US stimulation (0.15 ± 0.04; $p < 0.05$), and significantly lower compared to the high-amplitude peaks induced by the US stimulation in the presence of BTNPs characterized by a tetragonal crystalline structure ($p < 0.05$).

A representative Ca^{2+} imaging time-lapse frame is reported in the inlet of each graph of Figure 7, while more time-lapse images are provided in Figure S6 as Supporting Information. The XRD analysis of BTNPs characterized by a cubic crystalline structure is also reported in Supporting Information, as Figure S7.

DISCUSSION

Several *in vitro* studies have focused on the behavior of different cell types interacting with piezoelectric substrates/scaffolds. Detailed analysis of

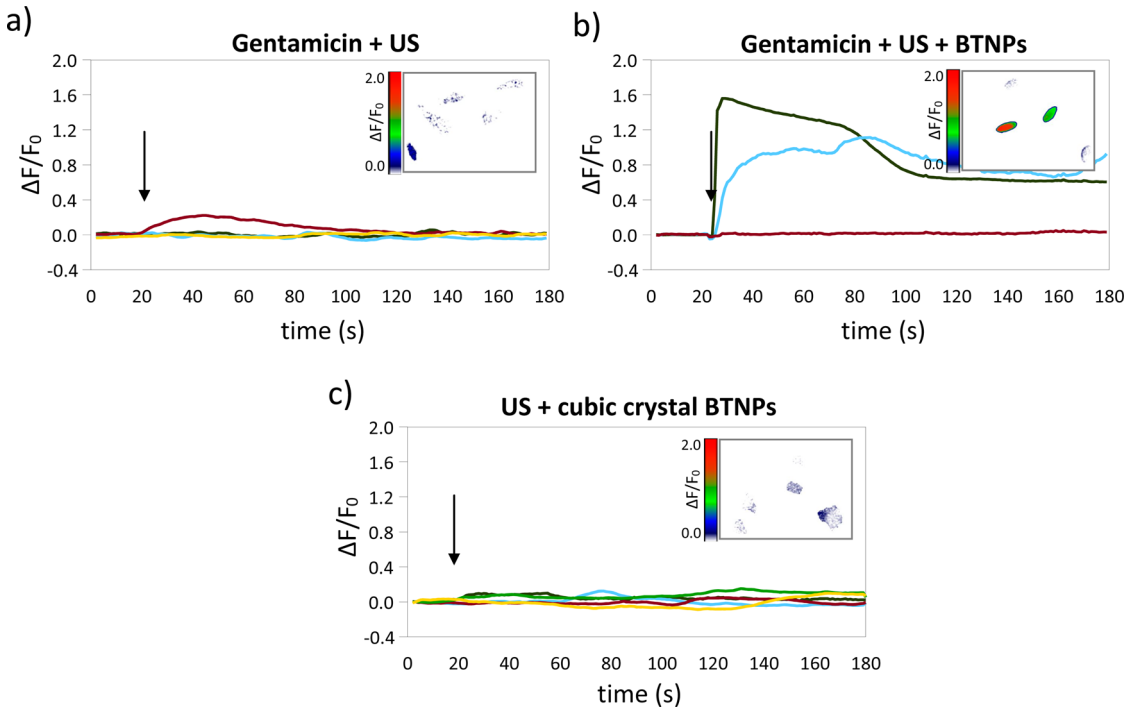

Figure 7. Calcium transients induced by US + BTNP stimulation (0.8 W/cm^2) are mediated by the piezoelectricity of the nanoparticles. Representative $\Delta F/F_0$ traces relative to calcium imaging time-lapses of SH-SY5Y-derived neurons stimulated by US (a) and US + BTNPs (b) in the presence of gentamicin, a blocker of mechano-sensitive cation channels which does not affect the voltage-gated Ca^{2+} currents. In (c) the Ca^{2+} time course of neurons stimulated by US and nonpiezoelectric BTNPs, characterized by a cubic crystalline configuration. Arrows indicate the moment when the 5-s US pulse was initiated; in the inlet of each graph a representative calcium imaging time-lapse frame is reported (at t = 50).

cytocompatibility and adhesion of human skin fibroblasts on electruspun poly(vinylidene fluoride-trifluoroethylene) (PVDF-TrFE) scaffolds have been for example carried out by the Arinzeh group.[36] In another work, Martins *et al.* investigated the biological effects of piezoelectric PVDF fiber polarization and alignment on the myoblast cell adhesion and morphology for muscles tissue engineering purposes.[37] Concerning neuron-piezoelectric substrate interactions, an interesting work of Lee *et al.* demonstrated the potential of micron-sized aligned PVDF-TrFE substrates in promoting and guiding the neurite outgrowth of dorsal root ganglion neurons.[38] These results are particularly interesting in view of exploiting piezoelectric substrates for promoting the neural tissue repair. Furthermore, in another work of the same group, the neural differentiation of human neural stem/progenitor cells (hNS/PCs) resulted significantly enhanced in terms of β-III tubulin positive cells and average neurite length when carried out on annealed (and thus characterized by improved piezoelectric properties) *vs* as-cast PVDF-TrFE scaffolds.[39] Obtained results were observed without making use of any mechanical stimulation, and authors hypothesized that fiber piezoelectricity was likely triggered by the forces exerted by the cells throughout adhesion and migration.[40] In other approaches, instead, piezoelectric PVDF scaffolds were able to generate an alternating electric field on their surfaces when mechanically deformed by a custom-made vibration base. A neurite length increase of rat spinal cord neurons was reported on stimulated piezoelectric PVDF substrates compared to nonpiezoelectric stimulated control scaffolds.[24] Alternatively, a dedicated device allowed to apply specific tension to the substrate by regulating the vacuum pressure in order to piezoelectrically stimulate fibroblasts cultured on polyurethane/PVDF scaffolds.[41] Finally, Inaoka *et al.* demonstrated as acoustic vibrations were also able to excite a piezoelectric membrane and, consequently, to generate electrical signals. The amplified signals were than transferred to the cochlea of deafened guinea pigs, so artificially mimicking the functions of the cochlear epithelium.[42]

In this work we successfully exploited for the first time piezoelectric BTNPs, characterized by a tetragonal crystalline configuration, for an US-driven piezoelectric stimulation of SH-SY5Y-derived neurons. Primarily, we observed as BTNPs functionalized with gum Arabic are associated with the plasma membrane of cells after 24 h of incubation. The observed low internalization of BTNPs is likely due to their negative external charge, which is known to limit the nanoparticle up-take.[43] However, the localization of the BTNPs at the neural plasma membrane, which is enriched of voltage-gated channels and it is electrically excitable, is optimal with the perspective of a piezoelectric stimulation.[44] The US + BTNP stimulation was able to activate high-amplitude Ca^{2+} transients, while the simple US stimulation, without BTNPs, induce low-amplitude Ca^{2+}

transients. The nonstereotyped amplitude and the duration (in the order of minute) of the transients observed after the US + BTNP stimulation suggest that these transient are Ca^{2+} waves.[45] These phenomena are known to be dependent on extracellular Ca^{2+} and mediated by voltage-gated Na^{+} and Ca^{2+} channels.[46,47] Furthermore, it is well-known from the literature as the Ca^{2+} waves, both spontaneous and stimuli-induced, intercellularly propagate through adjacent neurons thanks to gap junctions.[46] Interestingly, we found as some of the observed high-amplitude calcium transients do not occur simultaneously to the US + BTNP stimulation: a possible explanation of this phenomenon is related to the possibility that other activated neurons propagate the excitation to adjacent neurons. Calcium waves are known to play a key role in promoting the maturation of the neural network, especially by regulating the neurite outgrowth:[45] at this regard, it is worth to mention as we previously demonstrated how the US-driven stimulation of piezoelectric BNNTs was able to significantly promote the neurite elongation of PC12 neural-like cells, compared to the US control stimulation without BNNTs. In that work, it was hypothesized that Ca^{2+} influx was involved in the increase of the neurite outgrowth, since this was sensible to the nonspecific Ca^{2+} influx blockers. The findings presented in the current work are consistent with that hypothesis, having observed how an US-driven piezoelectric stimulation is able to induce calcium influx.

The high-amplitude Ca^{2+} transients recorded following the US + BTNP stimulation are sensitive to TTX and Cd^{2+} treatment, suggesting that both Na^{+} and Ca^{2+} voltage-gated channels are involved. In particular, it is possible to argue that the opening of voltage-gated Na^{+} channels induces a depolarization of the plasma membrane, thus activates the voltage-gated Ca^{2+} channels, and, finally, increases the cytoplasmic Ca^{2+} concentration:[48] indeed, the TTX + US + BTNP experiments revealed as the voltage-gated Ca^{2+} channels were not sufficient, alone, to evoke high-amplitude Ca^{2+} transients. The opening of these voltage-gated channels in response to the US + BTNP stimulus is supposed to induce, as final outcome, a depolarization of the neuronal plasma membrane.[49]

Since the voltage-gated channels are expressed on the plasma membrane, the extracellular Ca^{2+} influx is likely involved in the generation of the observed high-amplitude Ca^{2+} transients. The US + BTNP stimulation in Ca^{2+}-free conditions reveals a significant decrease of the Ca^{2+} transient amplitude, confirming the role of the extracellular Ca^{2+} influx. However, in these conditions, it is possible to detect low-amplitude transients, similar to those measured in response to the US stimulation in standard conditions (with 2 mM of extracellular Ca^{2+}), suggesting that a small component of the cytoplasmic Ca^{2+} increase is due to a release from intracellular Ca^{2+} stores. Moreover, it is also possible to detect similar low-amplitude Ca^{2+} transients in response to the simple US stimulation in Ca^{2+}-free conditions. These results suggest that the US stimulation without BTNPs is able to induce low-amplitude Ca^{2+} transients triggering a release from intracellular Ca^{2+} stores. By depleting the Ca^{2+} from ER and in extracellular Ca^{2+}-free conditions, it is possible to completely eliminate the Ca^{2+} transients in response to both US and to US + BTNPs. This finding confirms the contribution of the ER in the US-dependent increase of the cytoplasmic Ca^{2+} concentration.

In this context, it is well-known from the literature that US stimulations higher than 0.5 W/cm^2 can induce a temperature increase,[28,17,29] which results into Ca^{2+} transients upon Ca^{2+} release from ER.[30] Particularly, the temperature-dependent Ca^{2+} release from the ER is likely evoked by an imbalance between an increased SERCA pump activity[30,31,50] and a decreased open probability of IP_3R.[30,31,51,52] Interestingly, we noticed as the US stimulation was able to increase the ER temperature independently by the presence of BTNPs, suggesting a possible role of the temperature in the US-induced Ca^{2+} release from ER. Since there is not a significantly different temperature increment following the US and the US + BTNP stimulations, it is possible to confirm that the high-amplitude Ca^{2+} transients evoked by US + BTNPs are not caused by a temperature increment, but instead induced by the voltage-gated channel opening.

In order to assess whether the observed phenomena were actually ascribable to the piezoelectric properties of the nanoparticles, that act as nanotransducers by inducing the opening of the voltage-gated channels in response to the US stimulation, we performed analogue experiments with US + BTNPs characterized by a cubic crystalline configuration, thus not piezoelectric. Indeed, this stimulation was not able to induce high-amplitude Ca^{2+} transients, confirming that the piezoelectricity of the tetragonal BTNPs is a necessary requirement for eliciting the observed high-amplitude Ca^{2+} transients.

This hypothesis was corroborated by a simple electroelastic model of a BTNP subjected to US stimulation. In particular, the model provides the following expression for the maximum electric potential increment φ_R generated by the US on the BTNP surface ($r = R$) with respect to the stress-free condition:

$$\varphi_R \equiv -\frac{R(se_{rr} + 2e_{r\theta})}{s\varepsilon_{rr}}\left(\frac{p_{US}}{s\gamma + 2\alpha}\right) \qquad (1)$$

In eq 1, R denotes the radius, e_{rr} and $e_{r\theta}$ the piezoelectric coefficients, and ε_{rr} the dielectric constant of the BTNP. Moreover, α, γ and s are known expressions also depending on the elastic properties of the BTNP (namely the Young modulus and the Poisson ratio). Finally, p_{US} denotes the maximum pressure associated

with the US wave. The model derivation is fully detailed in the Section S1 of Supporting Information, and relevant parameter values are discussed/referenced therein. On the basis of eq 1, when stimulating with 0.1 W/cm^2 the maximum voltage is around 0.07 mV, yet it rises to 0.19 mV when operating with 0.8 W/cm^2. In light of the BTNP clusters on the cell membrane (clusters of about 10 BTNPs in average have been quantified from confocal images), when using 0.8 W/cm^2 the induced voltage of a few mV can locally affect channel open probability,[49] by superposition. Furthermore, this induced voltage can virtually redistribute the charges of the bivalent ions in correspondence of the external surface of the plasma membrane and, consequently, enhance the voltage sensitivity of the voltage-gated channels through a shift of the channel activation curves.[53] Differently, when using 0.1 W/cm^2, it is more difficult for the voltage to affect channel activation, even where the BTNPs cluster. The above model predictions are fully compatible with the experimental observations, and they quantitatively foster the hypothesis of BTNP-mediated, piezoelectric cell stimulation.

CONCLUSION

Successfully US-driven piezoelectric neural stimulation was performed by exploiting BTNPs, and the involved ion fluxes at the base of this phenomenon were fully described. The US + BTNP stimulation can be considered a novel tool for a wireless neural stimulation. Future works will be devoted to the functionalization of the BTNPs with specific molecules, in order to target nanoparticles to the membranes of specific cell types: cell type selectivity will be in fact fundamental envisaging *in vivo* wireless stimulations of different parts of the brain, and in order to foster peculiar cellular functions. Obtained results, collectively, open new intriguing perspectives not only in the field of neural prosthetics, but also in tissue engineering and biorobotics.

METHODS

BTNP Characterization. Barium titanate nanoparticles were purchased by Nanostructured & Amorphous Materials, Inc., Houston, TX (1144DY). Details of sample purity and composition, as provided by the supplier, include the following: BaO/TiO_2 0.999−1.001, purity 99.9%; APS 300 nm; SSA 3.5−3.7 m^2/g. X-ray diffraction (XRD) patterns were recorded using an X-ray powder diffractometer (Kristalloflex 810, Siemens) using Cu Kα radiation (λ = 1.5406 A) at a scanning rate of 0.016° s^{-1} with 2θ ranging in 10°−80° at a temperature of 25 °C.

For use in biological experiments, BTNPs were dispersed in aqueous environment through a noncovalent wrapping with gum Arabic (G9752 from Sigma-Aldrich). Briefly, 10 mg of nanoparticles and 10 mg of gum Arabic were mixed in 10 mL of phosphate buffered saline (PBS) solution. The samples were sonicated for 12 h with a Bransonic sonicator 2510, by using an output power of 20 W. The final product is a stable 1 mg/mL nanoparticle dispersion, that was appropriately diluted in cell culture medium for biological experiments. Obtained dispersion was characterized through scanning electron microscopy (SEM, Helios NanoLab 600i FIB/SEM, FEI) and transmission electron microscopy (TEM, Zeiss 902). Moreover, particle size distribution and *Z*-potential were analyzed with a Nano *Z*-Sizer 90 (Malvern Instrument), both in water and in experimental conditions (50 μg/mL of BTNPs in artificial cerebrospinal fluid, see in the following for details).

For a control experiment, analogous nanoparticles but with cubic crystal structure (1143DY, from Nanostructured & Amorphous Materials) were used following the same preparation procedures.

Cell Culture, Differentiation and BTNP Treatment. Human neuroblastoma-derived cells (SH-SY5Y, ATCC CRL-2266) were cultured in DMEM/F12 with 10% fetal bovine serum (FBS, Gibco), 100 U/mL penicillin, and 100 μg/mL streptomycin on 35 mm diameter μ-dishes (Ibidi) at a density of 20000 cell/cm^2, and subsequently differentiated toward neurons in DMEM with 1% FBS, 10 μM all-trans-retinoic acid, 100 U/mL penicillin, and 100 μg/mL streptomycin. After 4 days of differentiation, SH-SY5Y-derived neurons were treated for 24 h with BTNPs at the final concentration of 50 μg/mL in the differentiation medium. This nanoparticle concentration was previously tested on the SH-SY5Y cell line and was demonstrated to be not toxic by performing several independent biocompatibility investigations in terms of proliferation, metabolic activity, apoptosis detection and reactive oxygen species detection.[54] Control neurons were instead treated for 24 h with the differentiation medium and vehicle of the nanoparticles (50 μg/mL gum Arabic).

Further cell viability evaluations in the present experimental conditions were performed with WST-1 assay ((2-(4-iodophenyl)-3-(4-nitophenyl)-5-(2,4disulfophenyl)-2*H*-tetrazoilium monosodium salt, provided in a premix electrocoupling solution, BioVision) and propidium iodide staining, in order to respectively assess metabolic activity and membrane integrity after the stimulation procedures. More in details, cultures undergone the stimulation protocol (described in the next paragraph) were incubated for further 24 h, thereafter culture medium was replaced with a 1:11 premix:medium solution, and incubation performed for further 2 h. Finally, the absorbance was read at 450 nm with a microplate reader (Victor3, PerkinElmer). Membrane integrity evaluation following the stimulation procedure was performed by adding 1 μg/mL of propidium iodide (PI, Molecular Probes) during the application of the ultrasounds, and assessing the number of PI-positive cells over the total number of cells through fluorescence microscopy (TE2000U, Nikon).

The analysis of the nanoparticle localization was performed by confocal fluorescence microscopy (FluoView FV1000, PLAPON 60XO, NA1.42, Olympus). Neuronal plasma membranes and nuclei were stained with CellMask Green Plasma Membrane Stain (1:1000, Invitrogen) and Hoechst 33342 (1 μg/mL, Invitrogen), respectively. The ER staining in live cells was performed by using ER tracker Green (500 nM, Invitrogen) and ER thermo yellow[32] (300 nM). BTNPs, CellMask Green, Hoechst 33342, ER tracker Green and ER thermo yellow were excited by 633, 488, 405, 488, and 543 nm lasers, and the emission lights were collected at 645−745, 500−555, 425−525, 500−555 and 555−655 nm, respectively.

Ca^{2+}, Na^+ and Temperature Imaging during US Stimulation. Before the stimulation experiments, Fluo-4 AM (1 μM, Invitrogen), CoroNa Green AM (1 μM, Invitrogen) or the ER thermo yellow[32] (300 nM) were incubated in serum-free DMEM for 30 min at 37 °C. After the reagent incubation, samples were washed, supplied with artificial cerebrospinal fluid (aCSF, composition in mM: NaCl 140, KCl 5, $CaCl_2$ 2, $MgCl_2$ 2, HEPES 10, D-glucose 10; pH 7.4) and positioned on an inverted fluorescence microscope. Fluo-4 and ER thermo yellow were imaged with a microscope IX81 (Olympus) equipped with an objective UPLFLN 40XO, NA 1.3, and a cooled CCD camera (Cool SNAP HQ2, Photometrics)

by using 460−480HQ and 535−555HQ as excitation filters, DM485 and DM565HQ as dichroic mirrors, and 495−540HQ and 570−625HQ as emission filters, respectively (all from Olympus). CoroNa Green was imaged with a microscope IX83 (Olympus) equipped with an objective UPLFLN 40XO, NA 1.3, and an electron multiplying charge-coupled device camera (iXon3, Andor Technology) by using BP470−495, DM505, and BP510−550 as an excitation filter, a dichroic mirror and an emission filter, respectively (all from Olympus).

Concerning the temperature imaging experiments, calibration was performed by using a near-infrared laser (1064 nm) as previously described,[32] and a sensitivity of −2.0%/°C relative to room temperature (24 °C) was measured (please refer to Supporting Information, Figure S5, for the calibration curve).

Stimulation was carried out after waiting 20 min for the stabilization of the cell conditions after the medium change, and for allowing the full de-esterification of the AM groups. Ultrasounds were applied with a Sonitron GTS Sonoporation System (ST-GTS, Nepagene) equipped with a plane wave transducer module (PW-1.0−6 mm, 6 mm diameter tip, 1 MHz). The probe was vertically fixed at a distance of 5 mm from the cells, and the US stimulations were carried out for 5 s at different intensities (from 0.1 W/cm^2 to 0.8 W/cm^2).

During the stimulation experiments, cadmium chloride ($CdCl_2$ 100 μM, Sigma), tetrodotoxin (TTX, 100 nM, Tocris), ethylene glycol tetraacetic acid (EGTA, 5 mM, Dojindo Laboratories), thapsigargin (2 μM, Sigma) or gentamicin (200 μM, Invitrogen) were added to the aCSF (Ca^{2+}-free aCSF was used in the case of the EGTA experiments). Concerning the thapsigargin experiments, this reagent was also applied during the dye internalization process, in order to allow the complete release of Ca^{2+} from the ER, as previously reported.[55]

Image and Statistical Analysis. The fluorescence images acquired during the time lapses were analyzed with ImageJ software (http://rsbweb.nih.gov/ij/). Images were thresholded in order to define the region of interest (ROI) to analyze; subsequently, they were converted in $\Delta F/F_0$ by using the divide and subtract functions of the Math process. After a double smoothing, the average values of the pixels inside the ROIs were measured by using the multimeasure function of the ROI manager and, finally, plotted on the $\Delta F/F_0$ graphs. Transient amplitudes ($\Delta F/F_0$ peaks) 3-fold higher than the standard deviation of the noise were reported in terms of peak average ± standard error.

All the described experiments were carried out in triplicate (at least the response of 20 cells for all the conditions was analyzed), the normality of all the data distributions was tested with the Shapiro normality test and, subsequently, the ANOVA parametric test followed by Tukey's HSD *post-hoc* test was performed in order to compare the different distributions.

Conflict of Interest: The authors declare no competing financial interest.

Acknowledgment. The authors gratefully thank Mr. Piero Narducci (Department of Chemical Engineering, University of Pisa, Pisa, Italy) for XRD technical assistance. This research was partially supported by the JSPS KAKENHI Grant Number 26107717 (to M.S.), by the JSPS Core-to-Core Program, A. Advanced Research Networks (to M.S.), and by the Italian Ministry of Health Grant Number RF-2011-02350464 (to G.C.).

Supporting Information Available: Section S1 contains an electroelastic model of the voltage generated by a piezoelectric BTNP subjected to ultrasounds. Figure S1 reports cell viability data following treatment with BTNPs and US. Figures S2, S3, S4 and S6 report time-lapse frames of the $\Delta F/F_0$ traces reported in Figures 4, 5, 6 and 7, respectively. Figure S5 shows the ER temperature imaging performed during the US (0.8 W/cm^2) and BTNP + US (0.8 W/cm^2) stimulations. Figure S7 reports the XRD analysis of BTNPs characterized by a cubic crystalline structure. Video S1 shows the confocal *z*-stack 3D rendering of a cluster of cells (plasma membrane in green, nuclei in blue) and BTNPs (in red) associated with their plasma membrane. Video S2 shows a Ca^{2+} imaging time-lapse course (18X accelerated) performed on cultures stimulated with US (0.8 W/cm^2) in the presence of BTNPs. The Supporting Information is available free of charge on the ACS Publications website at DOI: 10.1021/acsnano.5b03162.

REFERENCES AND NOTES

1. Chang, J.-Y. Brain Stimulation for Neurological and Psychiatric Disorders, Current Status and Future Direction. *J. Pharmacol. Exp. Ther.* **2004**, *309*, 1–7.
2. Deisseroth, K. Optogenetics. *Nat. Methods* **2011**, *8*, 26–29.
3. Gradinaru, V.; Mogri, M.; Thompson, K. R.; Henderson, J. M.; Deisseroth, K. Optical Deconstruction of Parkinsonian Neural Circuitry. *Science* **2009**, *324*, 354–359.
4. Tye, K. M.; Prakash, R.; Kim, S.-Y.; Fenno, L. E.; Grosenick, L.; Zarabi, H.; Thompson, K. R.; Gradinaru, V.; Ramakrishnan, C.; Deisseroth, K. Amygdala Circuitry Mediating Reversible and Bidirectional Control of Anxiety. *Nature* **2011**, *471*, 358–362.
5. Witten, I. B.; Lin, S.-C.; Brodsky, M.; Prakash, R.; Diester, I.; Anikeeva, P.; Gradinaru, V.; Ramakrishnan, C.; Deisseroth, K. Cholinergic Interneurons Control Local Circuit Activity and Cocaine Conditioning. *Science* **2010**, *330*, 1677–1681.
6. Chaudhury, D.; Walsh, J. J.; Friedman, A. K.; Juarez, B.; Ku, S. M.; Koo, J. W.; Ferguson, D.; Tsai, H.-C.; Pomeranz, L.; Christoffel, D. J.; *et al.* Rapid Regulation of Depression-Related Behaviours by Control of Midbrain Dopamine Neurons. *Nature* **2013**, *493*, 532–536.
7. Knöpfel, T.; Lin, M. Z.; Levskaya, A.; Tian, L.; Lin, J. Y.; Boyden, E. S. Toward the Second Generation of Optogenetic Tools. *J. Neurosci.* **2010**, *30*, 14998–15004.
8. Diester, I.; Kaufman, M. T.; Mogri, M.; Pashaie, R.; Goo, W.; Yizhar, O.; Ramakrishnan, C.; Deisseroth, K.; Shenoy, K. V. An Optogenetic Toolbox Designed for Primates. *Nat. Neurosci.* **2011**, *14*, 387–397.
9. Stanley, S. A.; Gagner, J. E.; Damanpour, S.; Yoshida, M.; Dordick, J. S.; Friedman, J. M. Radio-Wave Heating of Iron Oxide Nanoparticles Can Regulate Plasma Glucose in Mice. *Science* **2012**, *336*, 604–608.
10. Perlmutter, J. S.; Mink, J. W. Deep Brain Stimulation. *Annu. Rev. Neurosci.* **2006**, *29*, 229–257.
11. Brunoni, A. R.; Nitsche, M. A.; Bolognini, N.; Bikson, M.; Wagner, T.; Merabet, L.; Edwards, D. J.; Valero-Cabre, A.; Rotenberg, A.; Pascual-Leone, A.; *et al.* Clinical Research with Transcranial Direct Current Stimulation (tDCS): Challenges and Future Directions. *Brain Stimulat.* **2012**, *5*, 175–195.
12. Stagg, C. J.; Nitsche, M. A. Physiological Basis of Transcranial Direct Current Stimulation. *Neuroscientist* **2011**, *17*, 37–53.
13. Hallett, M. Transcranial Magnetic Stimulation and the Human Brain. *Nature* **2000**, *406*, 147–150.
14. Tufail, Y.; Matyushov, A.; Baldwin, N.; Tauchmann, M. L.; Georges, J.; Yoshihiro, A.; Tillery, S. I. H.; Tyler, W. J. Transcranial Pulsed Ultrasound Stimulates Intact Brain Circuits. *Neuron* **2010**, *66*, 681–694.
15. Li, J.; Fok, L.; Yin, X.; Bartal, G.; Zhang, X. Experimental Demonstration of an Acoustic Magnifying Hyperlens. *Nat. Mater.* **2009**, *8*, 931–934.
16. Zhang, S.; Yin, L.; Fang, N. Focusing Ultrasound with an Acoustic Metamaterial Network. *Phys. Rev. Lett.* **2009**, *102*, 194301.
17. Tufail, Y.; Yoshihiro, A.; Pati, S.; Li, M. M.; Tyler, W. J. Ultrasonic Neuromodulation by Brain Stimulation with Transcranial Ultrasound. *Nat. Protoc.* **2011**, *6*, 1453–1470.
18. Wang, X.; Song, J.; Liu, J.; Wang, Z. L. Direct-Current Nanogenerator Driven by Ultrasonic Waves. *Science* **2007**, *316*, 102–105.
19. Qin, Y.; Wang, X.; Wang, Z. L. Microfibre−nanowire Hybrid Structure for Energy Scavenging. *Nature* **2008**, *451*, 809–813.
20. Wang, X.; Liu, J.; Song, J.; Wang, Z. L. Integrated Nanogenerators in Biofluid. *Nano Lett.* **2007**, *7*, 2475–2479.
21. Kim, K.-H.; Kumar, B.; Lee, K. Y.; Park, H.-K.; Lee, J.-H.; Lee, H. H.; Jun, H.; Lee, D.; Kim, S.-W. Piezoelectric Two-Dimensional Nanosheets/anionic Layer Heterojunction for Efficient Direct Current Power Generation. *Sci. Rep.* **2013**, 10.1038/srep02017.
22. Zhao, Y.; Liao, Q.; Zhang, G.; Zhang, Z.; Liang, Q.; Liao, X.; Zhang, Y. High Output Piezoelectric Nanocomposite

Generators Composed of Oriented $BaTiO_3$ NPs@PVDF. *Nano Energy* **2015**, *11*, 719–727.
23. Ciofani, G.; Danti, S.; D'Alessandro, D.; Ricotti, L.; Moscato, S.; Bertoni, G.; Falqui, A.; Berrettini, S.; Petrini, M.; Mattoli, V.; *et al.* Enhancement of Neurite Outgrowth in Neuronal-Like Cells Following Boron Nitride Nanotube-Mediated Stimulation. *ACS Nano* **2010**, *4*, 6267–6277.
24. Royo-Gascon, N.; Wininger, M.; Scheinbeim, J. I.; Firestein, B. L.; Craelius, W. Piezoelectric Substrates Promote Neurite Growth in Rat Spinal Cord Neurons. *Ann. Biomed. Eng.* **2013**, *41*, 112–122.
25. Tao, J.; Ma, J.; Wang, Y.; Zhu, X.; Liu, J.; Jiang, X.; Lin, B.; Ren, Y. Synthesis of Barium Titanate Nanoparticles *via* a Novel Electrochemical Route. *Mater. Res. Bull.* **2008**, *43*, 639–644.
26. Lee, C. H.; Ruben, P. C. Interaction between Voltage-Gated Sodium Channels and the Neurotoxin, Tetrodotoxin. *Channels* **2008**, *2*, 407–412.
27. Lacinová, L. Voltage-Dependent Calcium Channels. *Gen. Physiol. Biophys.* **2005**, *24* (Suppl 1), 1–78.
28. Ter Haar, G. Therapeutic Applications of Ultrasound. *Prog. Biophys. Mol. Biol.* **2007**, *93*, 111–129.
29. O'Brien, W. D. Ultrasound—biophysics Mechanisms. *Prog. Biophys. Mol. Biol.* **2007**, *93*, 212–255.
30. Itoh, H.; Oyama, K.; Suzuki, M.; Ishiwata, S. Microscopic Heat Pulse-Induced Calcium Dynamics in Single WI-38 Fibroblasts. *Biophysics* **2014**, *10*, 109–119.
31. Tseeb, V.; Suzuki, M.; Oyama, K.; Iwai, K.; Ishiwata, S. Highly Thermosensitive Ca2+ Dynamics in a HeLa Cell through IP3 Receptors. *HFSP J.* **2009**, *3*, 117–123.
32. Arai, S.; Lee, S.-C.; Zhai, D.; Suzuki, M.; Chang, Y. T. A Molecular Fluorescent Probe for Targeted Visualization of Temperature at the Endoplasmic Reticulum. *Sci. Rep.* **2014**, *4*, 6701.
33. Calabrese, B.; Manzi, S.; Pellegrini, M.; Pellegrino, M. Stretch-Activated Cation Channels of Leech Neurons: Characterization and Role in Neurite Outgrowth. *Eur. J. Neurosci.* **1999**, *11*, 2275–2284.
34. Barsanti, C.; Pellegrini, M.; Ricci, D.; Pellegrino, M. Effects of Intracellular pH and Ca^{2+} on the Activity of Stretch-Sensitive Cation Channels in Leech Neurons. *Pfluegers Arch.* **2006**, *452*, 435–443.
35. Jacques-Fricke, B. T.; Seow, Y.; Gottlieb, P. A.; Sachs, F.; Gomez, T. M. Ca^{2+} Influx through Mechanosensitive Channels Inhibits Neurite Outgrowth in Opposition to Other Influx Pathways and Release from Intracellular Stores. *J. Neurosci.* **2006**, *26*, 5656–5664.
36. Weber, N.; Lee, Y.-S.; Shanmugasundaram, S.; Jaffe, M.; Arinzeh, T. L. Characterization and in Vitro Cytocompatibility of Piezoelectric Electrospun Scaffolds. *Acta Biomater.* **2010**, *6*, 3550–3556.
37. Martins, P. M.; Ribeiro, S.; Ribeiro, C.; Sencadas, V.; Gomes, A. C.; Gama, F. M.; Lanceros-Méndez, S. Effect of Poling State and Morphology of Piezoelectric Poly(vinylidene Fluoride) Membranes for Skeletal Muscle Tissue Engineering. *RSC Adv.* **2013**, *3*, 17938–17944.
38. Lee, Y.-S.; Collins, G.; Arinzeh, T. L. Neurite Extension of Primary Neurons on Electrospun Piezoelectric Scaffolds. *Acta Biomater.* **2011**, *7*, 3877–3886.
39. Lee, Y.-S.; Arinzeh, T. L. The Influence of Piezoelectric Scaffolds on Neural Differentiation of Human Neural Stem/progenitor Cells. *Tissue Eng., Part A* **2012**, *18*, 2063–2072.
40. Wang, N.; Tolić-Nørrelykke, I. M.; Chen, J.; Mijailovich, S. M.; Butler, J. P.; Fredberg, J. J.; Stamenović, D.; Cell Prestress, I. Stiffness and Prestress Are Closely Associated in Adherent Contractile Cells. *Am. J. Physiol. Cell Physiol.* **2002**, *282*, C606–C616.
41. Guo, H.-F.; Li, Z.-S.; Dong, S.-W.; Chen, W.-J.; Deng, L.; Wang, Y.-F.; Ying, D.-J. Piezoelectric PU/PVDF Electrospun Scaffolds for Wound Healing Applications. *Colloids Surf., B* **2012**, *96*, 29–36.
42. Inaoka, T.; Shintaku, H.; Nakagawa, T.; Kawano, S.; Ogita, H.; Sakamoto, T.; Hamanishi, S.; Wada, H.; Ito, J. Piezoelectric Materials Mimic the Function of the Cochlear Sensory Epithelium. *Proc. Natl. Acad. Sci. U. S. A.* **2011**, *108*, 18390–18395.
43. Fröhlich, E. The Role of Surface Charge in Cellular Uptake and Cytotoxicity of Medical Nanoparticles. *Int. J. Nanomed.* **2012**, *7*, 5577–5591.
44. Armstrong, C. M.; Hille, B. Voltage-Gated Ion Channels and Electrical Excitability. *Neuron* **1998**, *20*, 371–380.
45. Rosenberg, S. S.; Spitzer, N. C. Calcium Signaling in Neuronal Development. *Cold Spring Harbor Perspect. Biol.* **2011**, *3*, a004259.
46. Charles, A. C.; Kodali, S. K.; Tyndale, R. F. Intercellular Calcium Waves in Neurons. *Mol. Cell. Neurosci.* **1996**, *7*, 337–353.
47. Gu, X.; Olson, E. C.; Spitzer, N. C. Spontaneous Neuronal Calcium Spikes and Waves during Early Differentiation. *J. Neurosci.* **1994**, *14*, 6325–6335.
48. Berridge, M. J.; Bootman, M. D.; Roderick, H. L. Calcium Signalling: Dynamics, Homeostasis and Remodelling. *Nat. Rev. Mol. Cell Biol.* **2003**, *4*, 517–529.
49. Catterall, W. A. Structure and Function of Voltage-Gated Ion Channels. *Annu. Rev. Biochem.* **1995**, *64*, 493–531.
50. Dode, L.; Van Baelen, K.; Wuytack, F.; Dean, W. L. Low Temperature Molecular Adaptation of the Skeletal Muscle Sarco(endo)plasmic Reticulum Ca2+-ATPase 1 (SERCA 1) in the Wood Frog (Rana Sylvatica). *J. Biol. Chem.* **2001**, *276*, 3911–3919.
51. Stavermann, M.; Buddrus, K.; St John, J. A.; Ekberg, J. A. K.; Nilius, B.; Deitmer, J. W.; Lohr, C. Temperature-Dependent Calcium-Induced Calcium Release *via* InsP3 Receptors in Mouse Olfactory Ensheathing Glial Cells. *Cell Calcium* **2012**, *52*, 113–123.
52. Dickinson, G. D.; Parker, I. Temperature Dependence of IP3-Mediated Local and Global Ca^{2+} Signals. *Biophys. J.* **2013**, *104*, 386–395.
53. Hille, B. *Modifiers of Gating*; Sinauer Associates Inc.: Sunderland, MA, 1992; Ionic Channels of Excitable Membranes, Vol. 17.
54. Ciofani, G.; Danti, S.; D'Alessandro, D.; Moscato, S.; Petrini, M.; Menciassi, A. Barium Titanate Nanoparticles: Highly Cytocompatible Dispersions in Glycol-Chitosan and Doxorubicin Complexes for Cancer Therapy. *Nanoscale Res. Lett.* **2010**, *5*, 1093.
55. Paschen, W.; Doutheil, J.; Gissel, C.; Treiman, M. Depletion of Neuronal Endoplasmic Reticulum Calcium Stores by Thapsigargin: Effect on Protein Synthesis. *J. Neurochem.* **1996**, *67*, 1735–1743.